

Measurement of mechanical tractions exerted by cells in three-dimensional matrices

Wesley R Legant¹, Jordan S Miller¹, Brandon L Blakely¹, Daniel M Cohen¹, Guy M Genin² & Christopher S Chen¹

Quantitative measurements of cell-generated forces have heretofore required that cells be cultured on two-dimensional substrates. We describe a technique to quantitatively measure three-dimensional traction forces exerted by cells fully encapsulated in well-defined elastic hydrogel matrices. Using this approach we measured traction forces for several cell types in various contexts and revealed patterns of force generation attributable to morphologically distinct regions of cells as they extend into the surrounding matrix.

Cells are constantly probing, pushing and pulling on the surrounding extracellular matrix. These cell-generated forces drive cell migration and tissue morphogenesis, and maintain the intrinsic mechanical tone of tissues^{1,2}. Such forces not only guide mechanical and structural events but also trigger signaling pathways that promote functions ranging from proliferation to stem-cell differentiation^{3,4}. Therefore, precise measurements of the spatial and temporal nature of these forces are essential to understanding when and where mechanical events come to play in both physiological and pathological settings.

Methods using planar elastic surfaces or arrays of flexible cantilevers have been used to map, with subcellular resolution, the forces that cells generate against their substrates^{1,5–7}. But many processes are altered when cells are removed from native three-dimensional (3D) environments and maintained on two-dimensional (2D) substrates. Cells encapsulated in a 3D matrix exhibit dramatically different morphology, cytoskeletal organization and focal adhesion structure from those on 2D substrates⁸. Even the initial means by which cells attach to and spread against a 2D substrate are quite different from the invasive process required for cells to extend inside a 3D matrix. These

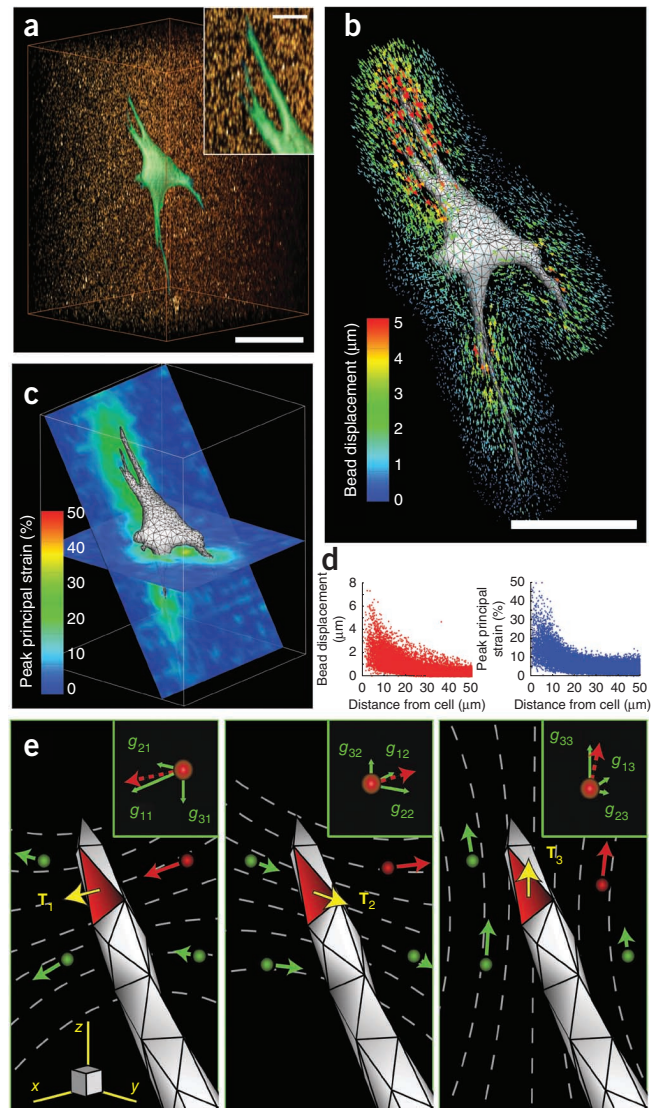
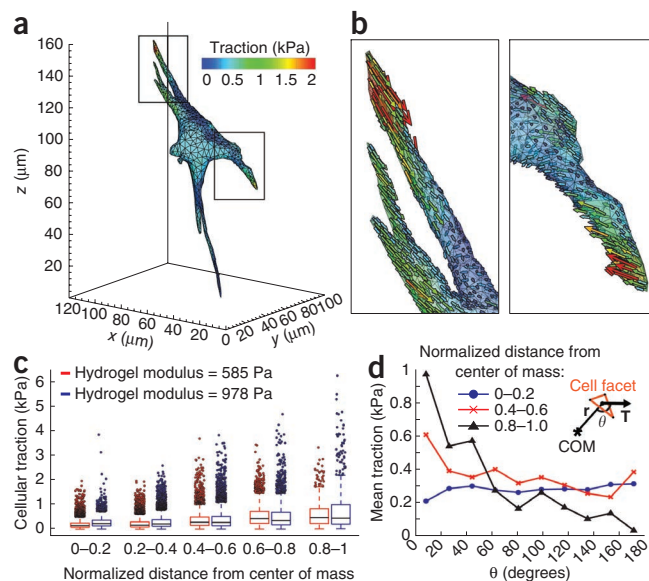


Figure 1 | Cell-induced hydrogel deformations and construction of a discretized Green's function. **(a)** Volume rendering of an EGFP-expressing NIH 3T3 fibroblast spreading into a 3D hydrogel containing fluorescent beads (red). Scale bar, 50 μm (10 μm in inset). **(b)** Bead displacement trajectories color coded by magnitude. Scale bar, 50 μm . **(c)** Two-dimensional slices through the volume showing the magnitude of the peak principal strain in the hydrogel surrounding the cell. **(d)** Plots of bead displacements and hydrogel strain as a function of distance from the cell surface. **(e)** Schematic outlining the use of the finite element method to reconstruct the Green's function. Surface traction (\mathbf{T}) applied to the highlighted facet induced displacements of the surrounding beads (g_{ij} ; inset). When repeated over all facets and beads, these relationships describe a discretized Green's function that can be used to calculate the tractions applied by the cell. The subscript indices of \mathbf{T} and g represent the Cartesian components of the bead displacement in direction i in response to an applied surface traction in direction j .

¹Department of Bioengineering, University of Pennsylvania, Philadelphia, Pennsylvania, USA. ²Department of Mechanical, Aerospace and Structural Engineering, Washington University in St. Louis, St. Louis, Missouri, USA. Correspondence should be addressed to C.S.C. (chriscchen@seas.upenn.edu).

RECEIVED 7 JULY; ACCEPTED 19 OCTOBER; PUBLISHED ONLINE 14 NOVEMBER 2010; DOI:10.1038/NMETH.1531

Figure 2 | Measurement of tractions exerted by live cells. **(a)** Contour plot of the tractions (magnitude) exerted by a cell. **(b)** Magnification of sections outlined in **a**, showing the individual traction vectors on each facet. **(c)** Boxplot of the traction magnitudes as a function of the normalized distance from the center of mass of the cell. This normalized distance was ~ 1 for the most spread regions (such as tips of long, slender extensions) and ~ 0 for the central cell body. **(d)** Mean traction at a given angle for cells encapsulated in 978 ± 228 Pa hydrogels. Inset, the angle (θ) was computed between the traction vector (\mathbf{T}) and the position vector (\mathbf{r}) of the cell facet with respect to the cell's center of mass (COM). Data shown in **c** and **d** are for 12 cells for each condition.



differences suggest that dimensionality alone may substantially impact how cellular forces are generated and transduced into biochemical or structural changes. Although the mechanical properties of 3D extracellular matrices and the cellular forces generated therein have been shown to regulate many cellular functions⁹, to our knowledge, cellular forces in a 3D context have yet to be quantitatively measured.

Here we quantitatively measure the traction stresses (force per area), hereafter referred to as ‘tractions’, exerted by cells embedded in a hydrogel matrix. We encapsulated enhanced GFP (EGFP)-expressing fibroblasts in mechanically well-defined polyethylene glycol (PEG) hydrogels that incorporate proteolytically degradable domains in the polymer backbone and pendant adhesive ligands¹⁰. Incorporation of adhesive and degradable domains permitted the cells to invade, spread and adopt physiologically relevant morphologies (Fig. 1a and Supplementary Movie 1). The hydrogels used in this study had a Young’s modulus of 600–1,000 Pa (Supplementary Fig. 1), a range similar to that of commonly used extracellular matrices such as reconstituted collagen or Matrigel and to *in vivo* tissues such as mammary and brain tissue^{11,12}. Cells in 3D PEG gels deformed the surrounding matrix, which we visualized by tracking the displacements of 60,000–80,000 fluorescent beads in the vicinity of each cell (Fig. 1b, Supplementary Fig. 2, Supplementary Note 1 and Supplementary Movie 2). We determined bead displacements relative to a reference stress-free state of the gel after lysing the cell with detergent (Supplementary Movie 3). Typically we observed deformations of 20–30% peak principal strain in much of the hydrogel surrounding the cell (Fig. 1c,d). The largest strains, up to 50%, occurred in the vicinity of long, slender extensions, which is consistent with observations of strong forces exerted by these regions on 2D substrates¹³. Because the mechanics of the PEG hydrogels showed no substantial dependence on strain or frequency (Supplementary Fig. 1), we used linear elasticity theory and the finite element method to determine the cellular tractions that would give rise to the measured bead displacements. Briefly, we generated a finite element mesh of the hydrogel surrounding the cell from confocal images. We constructed a discretized Green’s function by applying unit tractions to each facet on the surface of the cell mesh and solving the finite element equations to calculate the induced bead displacements (Fig. 1e). Standard regularization methods for ill-posed, overdetermined linear systems of equations were then used to compute the tractions exerted by the cell (Supplementary Note 2). The time required to calculate a single dataset was ~ 4.5 h using readily available computational equipment. However, we could reduce this dramatically by using a simplified finite element mesh of the cell and hydrogel. These lower-resolution datasets still captured the fundamental character of higher-resolution measurements (Supplementary Fig. 3).

To validate the approach and to characterize its spatial resolution, we used simulated traction fields (Supplementary Fig. 4). We measured experimental noise owing to bead displacements in cell-free regions of the hydrogel before and after detergent treatment, and measured surface discretization noise from multiple discretizations of the same cells. Then we superimposed these datasets onto the displacements generated by simulated loadings before traction reconstruction. In this setting, the percentage of traction recovered was proportional to the magnitude and characteristic length of the simulated loadings (defined as the average period of spatial oscillation). For all cases, the presence of noise reduced recovery accuracy by ~ 20 –30%. Despite these limitations, the recovered tractions still captured the essential periodic features of even the most spatially complex simulated loadings with characteristic lengths of spatial variation down to 10 μm .

We next calculated the tractions from live cells encapsulated in 3D hydrogels and found that cells exerted 100–5,000-Pa tractions, with strong forces located predominantly near the tips of long, slender extensions (Fig. 2a,b and Supplementary Movie 4). For all measurements, forces were in static equilibrium with a typical error of ~ 1 –5% of the total force applied by the cell. Subsequent analysis revealed that these tractions were minimally impacted by possible variations in local hydrogel mechanics or by uncertainty in the measured bead displacements (Supplementary Figs. 5 and 6). Previous measurements of cellular forces on 2D surfaces have generally been limited to shear loadings, although recent studies have measured small forces exerted normal to the planar surface as well^{14,15}. It is unclear, however, whether these relationships might be altered for cells inside a 3D matrix. Here we found that cells encapsulated in a 3D matrix predominantly exerted shear tractions, although small normal tractions were also present near the cell body. To determine whether patterns of force might be associated with specific cell regions, we quantified the magnitude and angle of tractions with respect to the center of mass of the cell. Generally, tractions increased as a function of distance from the center of mass (Fig. 2c). Cells encapsulated in hydrogels with a Young’s modulus of $\sim 1,000$ Pa generated stronger tractions than those in ~ 600 -Pa hydrogels. The observed differences in tractions were not due to an overall increase in total cellular contractility, as

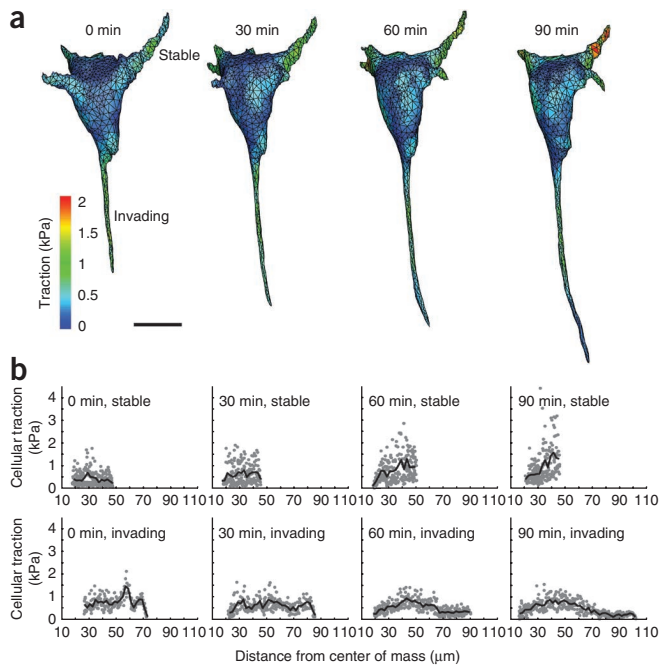


Figure 3 | Measurement of dynamic tractions exerted by spreading cells. (a) Contour plot of the tractions (magnitude) exerted by a cell as it invades into the surrounding hydrogel at indicated times relative to the beginning of measurement. Scale bar, 20 μm . (b) Tractions exerted by extensions labeled in a as a function of distance from the center of mass of the cell.

measured by the net contractile moment (Supplementary Fig. 7) but rather were most apparent in strong inward tractions near the tips of long, slender extensions (Fig. 2c). This reveals a local and nonlinear reinforcement of cellular contractility in response to substrate rigidity and suggests that such regions may be hubs for force-mediated mechanotransduction in 3D settings. The cell bodies showed no bias in traction angle, but strong tractions became progressively aligned back toward the center of mass in more well-spread regions of the cell (for example, near the tips of long, slender extensions) (Fig. 2d). In general, these patterns of force were reflected in multiple cell types but could be altered by cell-cell proximity or maintenance as a multicellular aggregate. Neighboring NIH 3T3 cells preferentially extended away from each other, whereas proliferating multicellular tumor spheroids exerted outward normal tractions on the matrix (Supplementary Figs. 8 and 9).

Upon closer inspection we found a subset of extensions that displayed strong tractions several micrometers behind the leading tip, whereas the tractions at the tip itself were substantially lower. As such traction profiles are similar to those observed behind the leading edge of a lamellipodia for a migrating cell on a 2D substrate¹, we hypothesized that such regions may represent invading or growing cellular extensions in three dimensions. To test this possibility, we measured the tractions from time-lapse images of cells as they invaded the surrounding hydrogel (Fig. 3a). Indeed, tractions at the tips of growing extensions were notably lower than the strong tractions exerted by proximal regions of the same extension (Fig. 3b and Supplementary Fig. 10). However, we did not observe normal forces pushing into the extracellular matrix in these extensions, which suggests that

a local inhibition of myosin-generated contractility allows tip advancement. Moreover, we also detected strong tractions from small extensions on the cell face opposite the invading extensions. Such stable extensions exhibited very different force distributions than the growing extensions, often lacking the characteristic drop in force near the leading edge, and may correspond to an anterior-posterior polarity axis formed in the cell.

These data suggest that cells in 3D matrices probe the surrounding extracellular matrix primarily through strong inward tractions near the tips of long, slender extensions. This technique was generalizable to different cell types, cell-cell interactions and even to multicellular tumor structures in which both tumor growth and invasion have been previously shown to be mechanoresponsive¹¹. Because the synthetic hydrogels used in this study had similar elastic moduli to *in vivo* tissues^{11,12} and can support many cellular functions¹⁶, we anticipate that this approach will enable investigations into the role of cellular forces in various biological settings.

METHODS

Methods and any associated references are available in the online version of the paper at <http://www.nature.com/naturemethods/>.

Note: Supplementary information is available on the Nature Methods website.

ACKNOWLEDGMENTS

We thank J. Baranski, H. Hu, C. Shen and M. Wozniak for helpful discussions. This work was supported in part by grants from the US National Institutes of Health (EB00262, EB08396, GM74048, HL73305 and HL90747), the Resbio Technology Resource for Polymeric Biomaterials, the Material Research Science and Engineering Center and Center for Engineering Cells and Regeneration at the University of Pennsylvania, the National Science Foundation graduate research fellowship (W.R.L. and B.L.B.), the US National Institutes of Health T32 training grant and the Hartwell Foundation (J.S.M.).

AUTHOR CONTRIBUTIONS

W.R.L., G.M.G. and C.S.C. conceived and initiated the project. W.R.L., J.S.M., B.L.B. and D.M.C. designed and performed experiments. C.S.C. supervised the project.

COMPETING FINANCIAL INTERESTS

The authors declare no competing financial interests.

Published online at <http://www.nature.com/naturemethods/>.

Reprints and permissions information is available online at <http://npg.nature.com/reprintsandpermissions/>.

- Dembo, M. & Wang, Y.L. *Biophys. J.* **76**, 2307–2316 (1999).
- Keller, R., Davidson, L.A. & Shook, D.R. *Differentiation* **71**, 171–205 (2003).
- Huang, S., Chen, C.S. & Ingber, D.E. *Mol. Biol. Cell* **9**, 3179–3193 (1998).
- McBeath, R., Pirone, D.M., Nelson, C.M., Bhadriraju, K. & Chen, C.S. *Dev. Cell* **6**, 483–495 (2004).
- Balaban, N.Q. *et al. Nat. Cell Biol.* **3**, 466–472 (2001).
- Butler, J.P., Tolic-Norrelykke, I.M., Fabry, B. & Fredberg, J.J. *Am. J. Physiol. Cell Physiol.* **282**, C595–C605 (2002).
- Tan, J.L. *et al. Proc. Natl. Acad. Sci. USA* **100**, 1484–1489 (2003).
- Cukierman, E., Pankov, R., Stevens, D.R. & Yamada, K.M. *Science* **294**, 1708–1712 (2001).
- Pampaloni, F., Reynaud, E.G. & Stelzer, E.H. *Nat. Rev. Mol. Cell Biol.* **8**, 839–845 (2007).
- Miller, J.S. *et al. Biomaterials* **31**, 3736–3743 (2010).
- Paszek, M.J. *et al. Cancer Cell* **8**, 241–254 (2005).
- Discher, D.E., Janmey, P. & Wang, Y.L. *Science* **310**, 1139–1143 (2005).
- Chan, C.E. & Odde, D.J. *Science* **322**, 1687–1691 (2008).
- Maskarinec, S.A., Franck, C., Tirrell, D.A. & Ravichandran, G. *Proc. Natl. Acad. Sci. USA* **106**, 22108–22113 (2009).
- Hur, S.S., Zhao, Y., Li, Y.S., Botvinick, E. & Chien, S. *Cell. Mol. Bioeng.* **2**, 425–436 (2009).
- Lutolf, M.P. & Hubbell, J.A. *Nat. Biotechnol.* **23**, 47–55 (2005).

ONLINE METHODS

Hydrogel synthesis and cell encapsulation. Polyethylene glycol diacrylate (PEGDA) was synthesized from PEG (molecular weight (MW), 3400; Sigma) and then modified with the collagenase-sensitive peptide CGPQGIWGQGCR to make degradable photoactive hydrogel precursors as described previously¹⁰. Polyethylene glycol diacrylamide (PEGDAAm; MW, 3400) was synthesized from PEG by forming the dimesylate, then the diamine and finally the diacrylamide as described previously¹⁷. PEGDAAm was then reacted with the collagenase-sensitive peptide in sodium borate (100 mM, pH 9.0) until the product polydispersity matched that for PEGDA-peptide precursors. For encapsulation, NIH 3T3 cells were resuspended to a final concentration of 60,000 cells ml⁻¹ in a 10 or 11% (w/v) solution of degradable PEGDA-peptide macromer in PBS (pH 7.4) containing 1 μmol ml⁻¹ acrylate-PEG-CGRGDS, 0.5 mg ml⁻¹ Irgacure 2959 (Ciba) and two types of fluorescent beads (0.2 μm diameter, nonfunctionalized, yellow-green dyed (Polysciences) and 0.2 μm diameter, nonfunctionalized, suncoast yellow dyed (Bangs Labs)) at $\sim 3.75 \times 10^{10}$ beads ml⁻¹ each. Note that the pore size of the PEG gels was an order of magnitude smaller than the diameter of the beads used in this study¹⁸. Therefore, the beads were physically encapsulated in the hydrogel and did not diffuse. Bovine pulmonary artery smooth muscle cells, human mesenchymal stem cells and Lewis lung carcinoma cells were encapsulated in a 7% (w/v) solution of PEGDAAm-peptide macromer in PBS containing 5 μmol ml⁻¹ acrylate-PEG-CGRGDS, 5 μmol ml⁻¹ acrylate-PEG-CGRGES, 0.5 mg ml⁻¹ Irgacure 2959 and two types of fluorescent beads. Next, 20 μl of cell-laden prepolymer solution was pipetted onto coverslips (0 thickness; Fisher Scientific) that were functionalized with 3-(trimethoxysilyl)propyl methacrylate (Sigma) per the manufacturer's instructions. The solution was contained in annular molds made from poly(dimethyl siloxane) (PDMS; Dow Corning) and exposed to 200 mW cm⁻² (measured at 365 nm) UV light from an Omnicure S2000 (320–500 nm; EXFO) for a total of 3,000 mJ. After removing the PDMS mold, polymerized hydrogels, which now formed a cylindrical disc that was ~ 4 mm in diameter and 500 μm tall and were covalently linked to the coverslip along the bottom surface, were immersed in cell culture medium and incubated under standard growth conditions (37 °C, 5% CO₂) for 72 h.

Microscopy, image segmentation, finite element mesh generation and computational resources. Encapsulated cells were imaged with a 40×, 1.1 numerical aperture (NA), water-immersion objective (LD C-Apochromat; Carl Zeiss) attached to an Olympus IX71 inverted microscope equipped with a CSU10 spinning disc confocal scan head (Yokogawa Electric Corporation), live-cell incubator (Pathology Devices) and an Imagem 16-bit electron-multiplying charge-coupled device (EMCCD) camera (Hamamatsu Photonics). A 147 × 147 × 200 μm volume was imaged around each cell, which corresponded to voxel dimensions of 0.2841 × 0.2841 × 0.8 μm in both horizontal planes and the axial plane, respectively. After the stressed image was acquired, the cells were treated with 0.5% SDS (JT Baker), re-equilibrated for 45 min and then reimaged to acquire a reference image of the nonstressed hydrogel. This detergent was chosen so as to completely denature all cellular proteins, although in practice, more mild detergents or specific inhibitors of cytoskeletal contractility

could be used as well. Time-lapse datasets were acquired at 30-min intervals and 1-μm spacing in the axial plane. This temporal and spatial resolution was chosen so as to increase the image acquisition speed (~ 3 min of exposure per volume per cell) and to reduce phototoxicity. Images were saved in multipage TIFF format, imported into Amira (Visage Imaging) and manually segmented to identify the cell and the surrounding hydrogel. A 2D surface mesh of the cell was generated from the segmented image, simplified to the desired number of elements and smoothed using built-in functions. This mesh was then imported into Hypermesh (Altair) as a stereolithography file. To approximate an infinite medium, we generated a 400-μm cube centered on the cell, seeded the edges with nine nodes (element size of 50 μm), and generated a 2D quadrilateral surface mesh. Using these two surface meshes as a template, we then generated a 3D tetrahedral mesh (four-node linear tetrahedron elements 'C3D4' in Abaqus) of the enclosed volume. These meshes were then imported into Abaqus (Dassault Systèmes) for finite element analysis with the bottom surface of the cube fixed as a boundary constraint. Validity of the finite element approximation of an infinite medium was verified by fixing the top surface of the cube as an additional boundary constraint and showed no substantial difference in the recovered tractions. Unless otherwise mentioned, for all measurements, the cells were discretized using 2,000 linear elements. The center of mass of the cell was computed using the area-weighted centroids of each element on the 2D surface mesh of the cell. Renderings of cellular tractions were computed in Tecplot 360 (Tecplot Inc.), and contour plots were scaled such that $\sim 1\%$ of all elements on the cell were saturated. The deviation of the tractions fields from static equilibrium was assessed by summing the projection of the forces (tractions multiplied by facet area) on each facet of the cell along each Cartesian direction. All data presented in the manuscript were calculated using a Dell Precision T7400 workstation equipped with dual quad core Intel Xeon processors and 16 GB of RAM (**Supplementary Note 3**).

Mechanical characterization of hydrogel substrates. The shear modulus of swollen gels was obtained using an AR 2000 oscillating rheometer (TA Instruments) on a temperature-controlled Peltier plate at 37 °C and a 20-mm stainless steel plate with solvent trap geometry (TA Instruments). Cylindrical gel samples were created from 125 μl of identical precursor solution to that used for traction measurements, covalently linked to glass microscope slides treated with 3-(trimethoxysilyl)propyl methacrylate (Sigma) and then swollen in growth medium at 37 °C and 5% CO₂ for 72 h. Immediately before testing, the slides were removed from medium and carefully blotted dry with laboratory wipes. The heights and diameter of the swollen gels were measured with calipers and were typically ~ 0.5 -mm thick and had a ~ 19 -mm diameter. To prevent slipping, 400 grit, wet-dry sandpaper was sectioned to fully cover the geometry and attached with double-stick tape. The head was lowered to a gap corresponding to approximately 0.2 N of normal force. Three consecutive controlled oscillatory strain sweeps were performed from 0.1–50% radial strain with 30 linearly spaced measurements at 0.25 Hz (**Supplementary Fig. 1a**). After the strain sweeps, frequency sweeps were performed from 0.1–10 Hz, ten measurements per decade on a log scale, at 1% controlled strain (**Supplementary Fig. 1b**). These data were acquired for six independent samples from multiple experiments. The data

from the strain sweeps were averaged to yield a shear modulus of 196 ± 66 Pa, 328 ± 76 Pa and 267 ± 34 Pa (\pm s.d.) for 10% (w/v) PEGDA, 11% (w/v) PEGDA and 7% (w/w) PEGDAam hydrogels, respectively. These values were used to calculate Young's moduli of 585 ± 196 Pa, 978 ± 228 Pa and 796 ± 102 Pa (\pm s.d.; assuming a Poisson's ratio of 0.49; **Supplementary Fig. 1c**).

To characterize the validity of a homogeneous material assumption, cell-laden degradable matrices were prepared as described above, cultured for 72 h, labeled with Cell Tracker Red (Invitrogen) according to the manufacturer's instructions and then treated with 0.5% SDS. Nondegradable matrices were prepared in an identical manner using PEGDA (MW, 6000; Sigma) in absence of degradable peptides and measured after 48 h. These matrices were imaged before and after applying a uniform compression of approximately 5% strain using a microscope mounted micromanipulator pressed against a coverslip laid over the gel (**Supplementary Fig. 5a**), and bead displacements throughout the volume were computed between the unstressed and compressed images. A 3D tetrahedral mesh was constructed in the vicinity of a cell as described above, and nodal displacements of the boundary nodes were interpolated from the experimentally observed bead displacements. The forward finite element solution was then solved for static equilibrium under homogeneous or heterogeneous (that is, weakening near the cell) material assumptions, and predicted bead displacements in the simulated volume were compared to experimental observations.

Measurement of uncertainties in the displacement field and discretized cell surface, and validation using simulated data.

The errors of the displacement measurements were measured from bead displacements before and after treatment with 0.5% SDS in six separate regions of the gel that contained no cells from multiple experiments. These six datasets were used to accurately reflect our experimental bead distribution and displacement resolution in all numerical simulations. To determine the uncertainty in our discretization of the cell surface, two separate surfaces were generated (starting with raw confocal data, proceeding through manual image segmentation and finally to surface reconstruction) of seven cells from multiple experiments. The differences between the two surface meshes for each cell were computed by finding the minimal distance between the nodes of one surface and the closest plane of the alternate surface. To model the cell in our numerical analysis, we used a simplified geometry of a 50- μ m-diameter sphere meshed using 2,000 triangular elements and generated a 3D tetrahedral mesh as described above. We first tested our ability to recover a uniform traction of 183 Pa oriented in the outward normal direction on each facet. The forward solution for this loading was solved, and bead displacements were measured at the centroid locations of each bead for each of the six fields measured above, thus giving six separate datasets of simulated bead displacements. The tractions were recovered for each of these simulated displacement fields and compared to the applied loading (**Supplementary Notes 2 and 3**), thus giving a measurement of the mean error and deviation of the recovered tractions. To simulate the effect of bead displacement noise on the recovered tractions, the experimentally measured displacements from each of the six noise fields were superimposed on the displacement resulting from the simulated loadings, and the tractions were recomputed. To simulate the effect of surface

discretization error, for each node of our spherical surface mesh, we randomly sampled measurements of the surface discretization error (computed as described above). As the most accurate discretization can be expected to lie in between the two experimentally generated surfaces, the spatial coordinates of each node from our spherical mesh were shifted either in the inward or outward normal direction (chosen randomly) by one half the magnitude of the experimentally measured noise. The restriction of the noise to the normal directions was necessary to avoid element intersections. This procedure was repeated to generate six independent samples of the surface-discretization noise (that is, we generated six independent 'noisy' spherical surfaces) on which to recover tractions.

To test the spatial resolution of the recovery, we applied oscillatory loadings normal to the cell surface. The magnitudes of these loadings varied sinusoidally with respect to the spherical coordinate θ . Three loadings were chosen with peak amplitudes of ± 183 , ± 743 and ± 1467 Pa. The frequency of these loadings was then increased progressively from two to ten oscillations per 360°, and six separate measurements of the recovered tractions were obtained for each loading. The characteristic length of the simulated loadings was calculated as the average period of oscillation on the surface of the sphere. The relative error between the simulated and recovered loadings was computed by summing over all elements as:

$$\text{Relative error} = \frac{|\mathbf{T}_{\text{recovered}} - \mathbf{T}_{\text{simulated}}|^2}{|\mathbf{T}_{\text{simulated}}|^2} \quad (1)$$

where $\mathbf{T}_{\text{recovered}}$ and $\mathbf{T}_{\text{simulated}}$ are $n \times 3$ matrices containing the recovered and simulated tractions respectively, n is the number of facets used to discretize the cell and each row contains the Cartesian components of the traction computed at a given facet. In this manner, a value of 0 indicates perfectly recovered tractions, 1 indicates that the errors are of equal magnitude to the simulated loadings and a value of greater than 1 indicates that the errors are larger than the simulated loadings. For cases in which this value was 0–1, it was possible to express a percentage traction recovery as $(1 - \text{relative error}) \times 100$.

Cell culture. NIH 3T3 cells (American Type Culture Collection; ATCC) were maintained in high-glucose DMEM containing 10% bovine serum, 2 mM L-glutamine, 100 units ml⁻¹ penicillin and 100 mg ml⁻¹ streptomycin (all from Invitrogen). Cell culture medium was changed every 3 d. EGFP-lentiviral infection was carried out as described previously¹⁹. Human mesenchymal stem cells from Lonza and Lewis lung carcinoma (LLC) cells from ATCC were maintained in growth medium (low-glucose DMEM containing 10% FBS, 0.3 mg ml⁻¹ glutamine, 100 units ml⁻¹ streptomycin and 100 units ml⁻¹ penicillin). Immediately upon encapsulation of single LLC cells, the medium was supplemented with 50 ng ml⁻¹ of recombinant human hepatocyte growth factor (R&D systems) to drive proliferation and spheroid formation.

17. Elbert, D.L. & Hubbell, J.A. *Biomacromolecules* **2**, 430–441 (2001).
18. Raeber, G.P., Lutolf, M.P. & Hubbell, J.A. *Biophys. J.* **89**, 1374–1388 (2005).
19. Gao, L., McBeath, R. & Chen, C.S. *Stem Cells* **28**, 564–572 (2010).